Atomic resolution crystal structures of HIV-1 protease and mutants V82A and I84V with saquinavir

ARTICLE *in* PROTEINS STRUCTURE FUNCTION AND BIOINFORMATICS · APRIL 2007

Impact Factor: 2.63 · DOI: 10.1002/prot.21304 · Source: PubMed

8 AUTHORS, INCLUDING:

Yunfeng Tie
Centers for Disease Control and Prevention
17 PUBLICATIONS **673** CITATIONS

SEE PROFILE

Andrey Kovalevsky
Oak Ridge National Laboratory
133 PUBLICATIONS **2,728** CITATIONS

SEE PROFILE

József Tőzsér
University of Debrecen
124 PUBLICATIONS **2,693** CITATIONS

SEE PROFILE

PROTEINS: Structure, Function, and Bioinformatics 67:232–242 (2007)

Atomic Resolution Crystal Structures of HIV-1 Protease and Mutants V82A and I84V with Saquinavir

Yunfeng Tie,[1] Andrey Y. Kovalevsky,[2] Peter Boross,[3] Yuan-Fang Wang,[2] Arun K. Ghosh,[4,5] Jozsef Tozser,[3] Robert W. Harrison,[2,6] and Irene T. Weber[1,2]*

[1]*Department of Chemistry, Georgia State University, Atlanta, Georgia 30303*
[2]*Department of Biology, Georgia State University, Atlanta, Georgia 30303*
[3]*Department of Biochemistry and Molecular Biology, Faculty of Medicine, University of Debrecen, Debrecen, Hungary*
[4]*Department of Chemistry, Purdue University, West Lafayette, Indiana 47907*
[5]*Department of Medicinal Chemistry, Purdue University, West Lafayette, Indiana 47907*
[6]*Department of Computer Science, Georgia State University, Atlanta, Georgia 30303*

ABSTRACT **Saquinavir (SQV), the first antiviral HIV-1 protease (PR) inhibitor approved for AIDS therapy, has been studied in complexes with PR and the variants PR_{I84V} and PR_{V82A} containing the single mutations I84V and V82A that provide resistance to all the clinical inhibitors. Atomic resolution crystal structures (0.97–1.25 Å) of the SQV complexes were analyzed in comparison to the protease complexes with darunavir, a new drug that targets resistant HIV, in order to understand the molecular basis of drug resistance. PR_{I84V} and PR_{V82A} complexes were obtained in both the space groups $P2_12_12$ and $P2_12_12_1$, which provided experimental limits for the conformational flexibility. The SQV interactions with PR were very similar in the mutant complexes, consistent with the similar inhibition constants. The mutation from bigger to smaller amino acids allows more space to accommodate the large group at P1′ of SQV, unlike the reduced interactions observed in darunavir complexes. The residues 79–82 have adjusted to accommodate the large hydrophobic groups of SQV, suggesting that these residues are intrinsically flexible and their conformation depends more on the nature of the inhibitor than on the mutations in this region. This analysis will assist with development of more effective antiviral inhibitors. Proteins 2007;67:232–242.** © 2007 Wiley-Liss, Inc.

Key words: AIDS; protease inhibitor; darunavir; drug resistance

INTRODUCTION

HIV-1 protease (PR) inhibitors are valuable therapeutic agents for HIV/AIDS. PR inhibitors are generally used in combination with other anti-HIV drugs during HAART therapy, which significantly reduces the viral load and has dramatically extended the lifetime of infected people.[1] The majority of clinical PR inhibitors, like the first FDA-approved inhibitor, saquinavir (SQV), were designed to target wild-type PR. However, the virus rapidly develops resistance to drugs, which greatly reduces the effectiveness of long-term therapy.[2,3] Consequently, newer inhibitors including darunavir[4] have been designed to target resistant PR variants as well as wild-type enzyme.

SQV, the first of the PR inhibitors approved by the FDA, has been shown to inhibit HIV-1 replication in both acutely and chronically infected cells with EC_{50} values in the range of 1–30 n*M*.[5] Combinations of SQV with other PR inhibitors, such as amprenavir, atazanavir, or lopinavir, resulted in synergistic antiviral activity. In cell culture, SQV exhibited additive to synergistic effects against HIV-1 when used with reverse transcriptase inhibitors and without increased cytotoxicity.[6] However, the long-term therapeutic efficiency of all these drugs is limited by the rapid development of resistant mutants with reduced susceptibility.[2,3,7,8] Genotypic analysis of HIV-1 isolates with reduced susceptibility to SQV identified G48V and L90M as the primary resistance conferring mutations in the PR gene, and secondary mutations L10I/R/V, I54V/L, A71L/T, G73S, V77I, V82A, and I84V that contributed additional resistance to SQV.[9–11] The reduction in susceptibility to SQV of clinical isolates bearing substitutions G48V and L90M depends on the number of secondary mutations present. In general, higher levels of resistance are associated with greater numbers of mutations in association with either or both of the primary mutations G48V and L90M.[11]

Crystal structures of HIV-1 PR (reviewed in Ref. 12) have guided the design of antiviral PR inhibitors.[13] Inhibitors bind in the active site formed by both subunits in the enzymatically active dimer of HIV-1 PR. Our

Grant sponsor: National Institutes of Health; Grant numbers: GM062920, GM53386; Grant sponsor: Hungarian Science and Research Fund; Grant numbers: OTKA F35191, T43482.

The coordinates and structure factors have been deposited in the Protein Data Bank as 2NMW (PR/SQV), 2NMY (PR_{V82A}/SQV in space group $P2_12_12$), 2NMZ (PR_{V82A}/SQV in space group $P2_12_12_1$), 2NNK (PR_{T84V}/SQV in space group $P2_12_12_1$), 2NNP (PR_{I84V}/SQV in space group $P2_12_12_1$).

*Correspondence to: Irene T. Weber; 402 Kell Hall, 24 Peachtree Center Ave., Atlanta, GA 30303. E-mail: iweber@gsu.edu

Received 13 September 2006; Revised 11 October 2006; Accepted 18 October 2006

Published online 22 January 2007 in Wiley InterScience (www.interscience.wiley.com). DOI: 10.1002/prot.21304

research has focused on the comprehensive structural and kinetic analysis of resistant variants of HIV-1 PR in complexes with inhibitors, including peptide analogs, indinavir and darunavir (DRV or TMC114), or in the unliganded form.[14–20] Limited structural studies have been done on PR complexes with SQV. Only a few structures (wild-type PR,[21] the double mutants $PR_{D25N/V82A}$[22] and $PR_{G48V/L90M}$,[23] and the PR_{9X} mutant structure[24]) are available and they were refined at around 2.5 Å resolution. Therefore, we describe the atomic resolution structures of the SQV complexes with wild-type HIV-1 PR and mutants PR_{V82A} and PR_{I84V} containing the single substitutions of V82A and I84V, respectively. The PR_{V82A}/SQV structure was refined at 0.97 Å resolution, which is the highest resolution structure reported for this inhibitor complex. V82A and I84V are two particularly important mutations that are commonly observed in cross-resistant virus. They are associated with high-level drug resistance for almost all eight available PR inhibitors. PR_{V82A} occurs predominantly in HIV-1 isolates from patients receiving treatment with indinavir and ritonavir, and also from patients receiving prolonged therapy with SQV, following the development of the mutation G48V. PR_{I84V} has been reported in patients receiving indinavir, ritonavir, SQV, and amprenavir, and causes phenotypic and clinical resistance to each inhibitor. Previously, we reported the crystal structures of the PR_{V82A} and PR_{I84V} mutants in their complexes with peptide analogs,[20] indinavir,[18] and the new FDA-approved inhibitor darunavir.[19,25] Thus, the SQV complexes presented here provide a valuable reference for comparison with other drugs that inhibit PR. The comparison will help understand the structural advantages and disadvantages of different inhibitors and further improve the design of more efficient inhibitors for resistant HIV.

METHODS

Protein Expression, Purification, and Inhibition

The construction, expression, and purification of HIV-1 PR, PR_{V82A}, and PR_{I84V} was carried out as described elsewhere.[12,26,27] Mutations were confirmed by DNA sequencing and protein mass spectrometry.

The inhibition constants were determined by a fluorescence assay as described previously.[28] The substrate RE(Edans)SQNY*PIVRK(Dabcyl)R (synthesized by Dr. Ivo Blaha, Ferring Leciva, Prague) was used. About 10 μL of PR (final concentration of 7–12 n*M*) was mixed with 100 μL PNF buffer (250 m*M* phosphate buffer, pH 5.6, containing 500 m*M* NaCl, 1 m*M* EDTA, 5 m*M* DTT, and 5% glycerol), 2 μL dimethyl sulfoxide (DMSO) and preincubated at 37°C for 5 min. SQV was dissolved in DMSO. The reaction was initiated by adding 90 μL substrate (final concentration of 6 μ*M*). The mixture was assayed over 5 min for the increase in fluorescence, which was detected at 460 nm, using 355 nm excitation wavelength in a POLARstar OPTIMA microplate reader (BMG Labtechnologies Inc.). The inhibition curves were fit using SigmaPlot 8.0.2 (SPSS Inc.). Inhibition constants were obtained from the IC_{50} values estimated from a dose–response curve using the equation $K_i = (IC_{50} - 0.5[E])/(1 + [S]/K_m)$, where $[E]$ and $[S]$ are the PR and substrate concentrations, respectively. Compensation for the inner filter effect was performed as described previously.[28]

Crystallization and X-ray Data Collection

SQV was dissolved in DMSO and centrifuged briefly to remove any insoluble material. The PR or mutant was concentrated to about 5 mg/mL, and mixed with SQV in fivefold molar excess. The mixture was incubated at 4°C for an hour and then centrifuged. Crystals were grown by the hanging-drop vapor-diffusion method, using equal volumes of enzyme–SQV stock and reservoir solution. The reservoir solution for crystals with space group $P2_12_12$ contained combination of the following solutions: 0.1*M* sodium acetate buffer, pH 4.2–5.0, with precipitant of 0.4–1.2*M* sodium chloride, 5% DMSO, and 0–5% dioxane, while those for crystals in space group $P2_12_12_1$ were combinations of 0.1*M* citrate phosphate buffer, pH 5.0–6.4, precipitant of 15–40% saturated ammonium sulfate and 5% DMSO. Crystals of suitable size for X-ray diffraction were obtained in 1 week. The crystals were frozen in liquid nitrogen using 30% (v/v) glycerol as a cryoprotectant. X-ray diffraction data were collected at the SER-CAT beamline of the Advanced Photon Source, Argonne National Laboratory.

Data Processing and Refinement

The diffraction data were processed using the HKL 2000 package.[29] The structures were solved by molecular replacement using AMoRe,[30] and structure 1S6G as a starting model. The structures were refined using the program SHELXL,[31] and map display and refitting used the molecular graphics program O.[32] Solvent molecules were identified from the potential for hydrogen bonding, the coordination state, and interatomic distances, for molecules present in the crystallization conditions. Alternate conformations were modeled for amino acid residues, inhibitor, water, and other solvent molecules when observed in the $2F_o - F_c$ electron density map. Anisotropic B factors were applied. Hydrogen atoms were calculated in the last round of refinement by SHELXL. Structures were superimposed as described in Ref. [18]. Structural figures were made using Bobscript[33] and Weblab viewer (Molecular Simulations Inc.).

Comparison Between Structures in Two Space Groups $P2_12_12$ and $P2_12_12_1$

The torsion angles were calculated for each residue in the PR_{V82A}/SQV complex using SHELX and compared for the structures determined in the space groups $P2_12_12$ and $P2_12_12_1$. For the residues with alternate conformations, the conformation that was closer to that of the corresponding one in the other space group was selected for comparison. The data were then analyzed by

TABLE I. Crystallographic Data Statistics for PR-SQV Complexes

Protease	PR	PR_{V82A}	PR_{V82A}	PR_{I84V}	PR_{I84V}
Space group	$P2_12_12_1$	$P2_12_12$	$P2_12_12_1$	$P2_12_12$	$P2_12_12_1$
Unit cell dimensions (Å)					
a	52.10	59.99	51.13	58.58	51.05
b	59.78	87.46	58.59	86.00	58.88
c	62.49	47.19	61.61	45.83	61.50
Resolution range (Å) (final shell)	50–1.16 (1.20–1.16)	50–1.10 (1.14–1.10)	50–0.97 (1.00–0.97)	50–1.25 (1.29–1.25)	50–1.20 (1.24–1.20)
Unique reflections	67,949	95,683	109,869	64,831	59,108
R_{merge} (%) overall (final shell)	7.5 (34.8)	11 (36.0)	10 (25.1)	4.7 (50.6)	6.5 (36.4)
$\langle I/\sigma \rangle$ overall (final shell)	14.6 (3)	10.5 (2)	20.5 (4)	11.3 (2)	11.1 (2)
Data range for refinement (Å)	10–1.16	10–1.10	10–0.97	10–1.25	10–1.20
R_{work} (%)	0.13	0.15	0.12	0.15	0.15
R_{free} (%)	0.18	0.18	0.14	0.19	0.20
No. of waters (total occupancies)	185.5	217	182.2	166	138.2
Completeness (%) overall (final shell)	96.6 (72.6)	94.6 (64.5)	89.3 (53.8)	92.8 (61.7)	92.6 (64.3)
RMS deviation from ideality					
Bonds (Å)	0.017	0.020	0.016	0.013	0.013
Angle distance (Å)	0.041	0.045	0.035	0.033	0.033
Average *B*-factors (Å^2)					
Main chain	12.3	13.7	8.8	15.8	15.0
Side chain	17.6	19.5	13.3	21.7	21.9
Inhibitor	11.3	13.3	9.0	14.2	16.7
Solvent	33.4	35.2	22.1	30.4	28.8
Relative occupancy of inhibitor(s)	0.5/0.5	0.7/0.3	0.5/0.5	0.7/0.3	1

the position along the polypeptide chain and by the amino acid type.

RESULTS

SQV Inhibition of PR_{V82A} and PR_{I84V}

PR and the drug-resistant mutant PRs, PR_{V82A} and PR_{I84V}, catalyze the hydrolysis of the fluorescent substrate, a synthetic peptide[28] with sequence based on the HIV-1 MA-CA cleavage site in the Gag-Pol polyprotein, and their catalytic activities are competitively inhibited by SQV. Their saturation kinetics with the same fluorescence assay were published previously;[15] the k_{cat}/K_m values were similar for PR_{V82A} and PR, and lower for PR_{I84V} (65% of PR). Surprisingly, the K_i values measured for SQV were essentially the same for PR and the two mutants: 3.9 ± 0.8 n*M* for PR, 4.3 ± 0.7 n*M* for PR_{V82A}, and 4.3 ± 0.4 n*M* for PR_{I84V}. In contrast, most of the other clinical inhibitors showed significantly poorer inhibition of the PR_{V82A} and PR_{I84V} mutants relative to wild-type enzyme.[34,35] However, the similar K_i values are consistent with the rare appearance of mutations V82A or I84V, rather than L90M and G48V, in HIV clinical isolates exposed to SQV.[9–11]

Crystal Structures

The crystal structures of PR and drug-resistant mutants PR_{V82A} and PR_{I84V} have been determined in their complexes with the clinical inhibitor SQV. The crystallographic statistics are summarized in Table I. The PR/SQV structure was determined in the $P2_12_12_1$ space group, while the structures of the two mutants were determined in both the space groups $P2_12_12$ and $P2_12_12_1$ with two different unit cells. Each crystallographic asymmetric unit contains one PR dimer comprising residues 1–99 and 1′–99′. All structures were refined at resolutions of 0.97–1.25 Å and *R* factors of 0.12–0.15, including disordered residues, solvent molecules, anisotropic *B*-factors, and hydrogen atoms. The electron density was excellent for all the atoms and especially for the subatomic resolution structure of PR_{V82A}/SQV complex. SQV was observed in two alternate conformations in all structures as shown by the electron density map [Fig. 1(A)], except for the PR_{I84V}/SQV complex in the $P2_12_12_1$ space group. Alternate conformations were also observed for residues 79′–82′ [Fig. 1(B)], which have direct interactions with SQV in all structures in the $P2_12_12_1$ space group. Similar to our other PR–inhibitor structures,[15,19] the majority of residues with two alternate conformations had long side chains and were located at the surface of the protein, while others were hydrophobic amino acids forming the inhibitor binding site, including Val82 and Ile84. The average *B*-factors were low for protein and inhibitor atoms, and decreased for the higher resolution data. The *B*-factors were in the ranges of 8.8–15.8, 13.3–21.9, 8.7–16.7, and 22.1–35.2 Å^2 for protein main chain atoms, side chain atoms, SQV, and solvent atoms, respectively.

SQV, the Catalytic Triad, Flap Residues and 80s Loop Show Correlated Alternate Conformations at Subatomic Resolution

The atom positions are defined most accurately with the subatomic resolution data for the PR_{V82A}/SQV com-

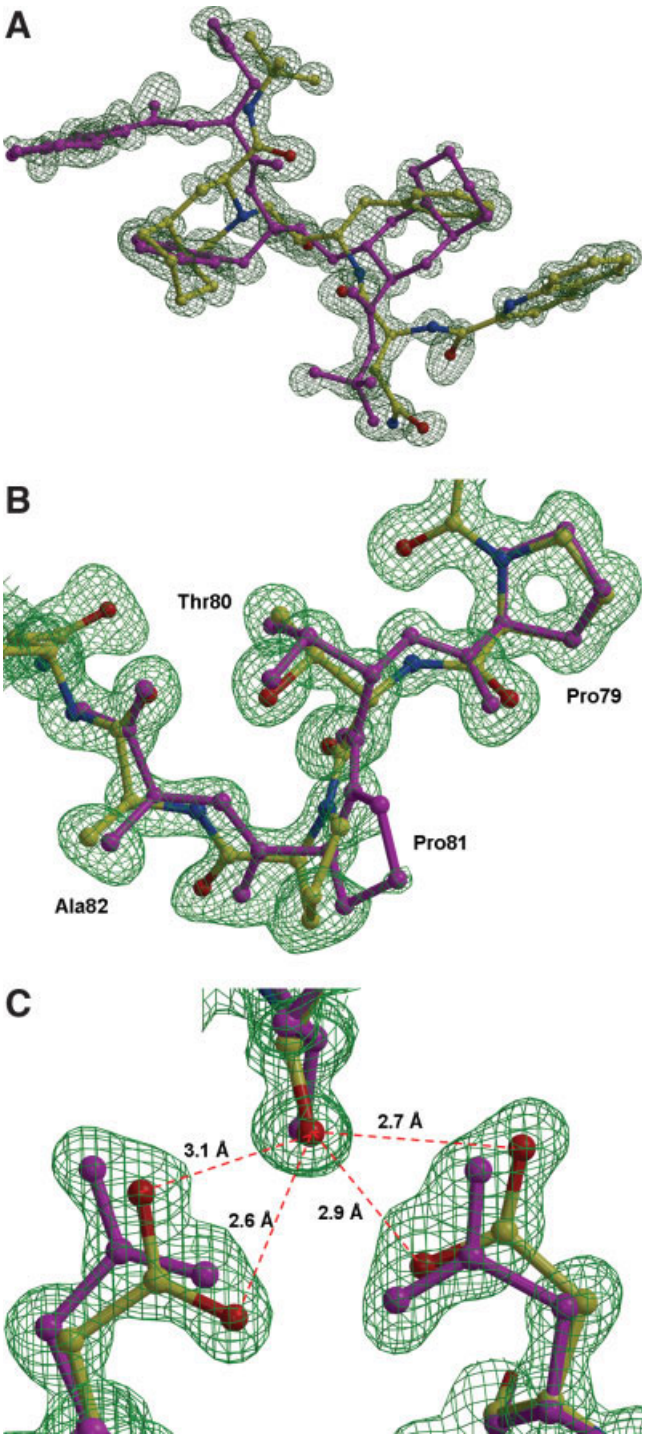

Fig. 1. The $2F_o - F_c$ electron density map for the crystal structure of PR_{V82A}/SQV. The major conformation is colored by atom type and the minor one is in magenta. (**A**) Saquinavir (contoured at 2.2σ level). (**B**) Residues 79–82 (contoured at 1.8σ level). (**C**) Catalytic site (contoured at 1.8σ level). Asp25 and 25′ are shown with the hydroxyl group of SQV.

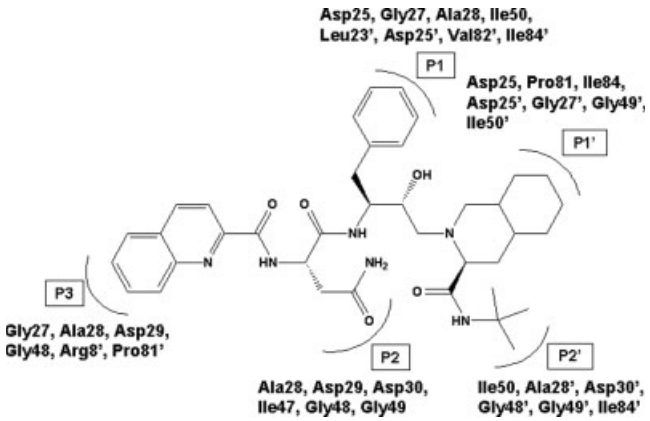

Fig. 2. SQV structure and PR residues forming van der Waals contacts.

plex in the $P2_12_12_1$ space group. Residues 24–26 and 24′–26′ around the catalytic Asp25/25′ showed two alternate conformations with the occupancy distribution of 0.55 and 0.45 [Fig. 1(C)], just as for SQV [Fig. 1(A)], which suggested a correlation between the alternate conformations of the active site residues and the SQV. After refinement with the two conformations, the partial positive and negative $F_o - F_c$ density around the catalytic triad disappeared. The hydroxyl group of the SQV formed hydrogen bonds with the carboxylate oxygens of Asp25 and Asp 25′ [Fig. 1(C)]. The other conformation of the inhibitor and catalytic residues had the same arrangement and distances. These more precise atomic positions of the active site residues may have not been correctly modeled before in other structures with two conformations of inhibitor. Thus, the subatomic resolution data have more accurately described the detailed geometry of the PR active site.

The tips of the flaps, residues 48–52 and 48′–52′, were also modeled with two conformations with the same relative occupancy as that of SQV. The major orientation of the flap residues was correlated with the major conformation of SQV, while the minor one correlated with the minor conformation of SQV. The main chain peptide group of Ile50/50′ had two conformations related by a 180° flip, and also the backbone of the flap residues 48–52/48′–52′ was moved about 0.2 Å to provide more space for the big P1′ ring of SQV.

The third region with alternate conformations was the 80s loop in both subunits (residues 79–82 and 79′–82′), as shown in Figure 1(B). In the PR/SQV and PR_{I84V}/SQV structures (in the $P2_12_12_1$ space group), the alternative conformations were observed only in one subunit for residues 79′–82′. Since this region plays an important role in binding the inhibitor, it will be further discussed later.

PR Interactions With SQV

SQV is a peptide-like inhibitor containing the main chain amides and carbonyl oxygen atoms of a peptide and a variety of groups corresponding approximately to the side chains at positions P3–P2′ of a peptide substrate (see Fig. 2). The large, hydrophobic groups at positions P3, P1, and P1′ of SQV lie in the hydrophobic

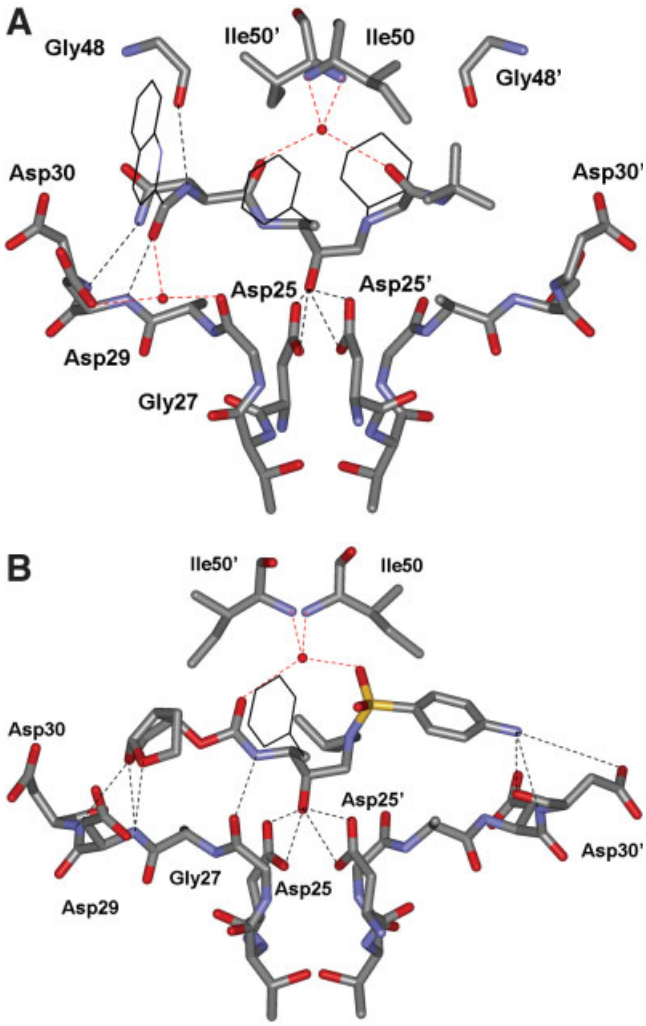

Fig. 3. Hydrogen bond interactions between PR and inhibitor. Hydrogen bond interactions are indicated by dashed lines. Interactions mediated by water are shown in red. (**A**) Hydrogen bond interactions between PR and SQV. (**B**) Hydrogen bond interactions between PR and darunavir. [Color figure can be viewed in the online issue, which is available at www.interscience.wiley.com.]

pockets S3, S1, and S1′ formed by the PR. There is a smaller hydrophobic *t*-butyl group at P2′ and the polar asparagine side chain at P2 of SQV. The P1 and P1′ groups of SQV formed van der Waals interactions with PR residues Leu23′, Asp25/25′, Gly27, Ala28, Gly49′, Ile50, Thr80, Pro81, Val82′, and Ile84/84′. The other groups of SQV interacted with residues Gly27, Ala28/28′, Asp29, Asp30/30′, Gly48/48′, Gly49/49′, Ile50, Pro81′, and Ile84′. The residues 79′–82′ in the PR/SQV structure interact closely with the SQV and showed alternate positions with the occupancy distribution of 0.7 and 0.3. Therefore, the flexibility of this region allows the PR to adapt to various subgroups on the different inhibitors.

The PR hydrogen bond interactions with SQV are shown in Figure 3(A). Seven direct hydrogen bonds are formed between PR and SQV. Four hydrogen bonds are formed between the hydroxyl group of SQV and the side chain carboxylate oxygen atoms of the catalytic Asp25/25′, and the other three are from O1 of SQV to the main chain amide of Asp29, from N3 to the amide nitrogen of Asp30, and from N3 to the main chain carbonyl oxygen of Gly48. Two water molecules mediated three more hydrogen bond interactions between PR and inhibitor. The conserved water linked the PR flaps and SQV, and the other water mediated the interactions between O1 of SQV and the main chain oxygen of Gly27 and side chain oxygen of Asp29. Both conformations of SQV showed a similar hydrogen bond network.

Comparison of the Structures of PR and Mutants

The three structures in the same space group of $P2_12_12_1$ were very similar overall, with calculated RMS deviations of 0.43 and 0.41 Å for Cα atoms in PR_{V82A} and PR_{I84V}, respectively, compared with PR. SQV was bound in two conformations in all complexes, except for PR_{I84V}/SQV in the $P2_12_12_1$ space group (Table I). SQV has very similar conformation and interactions in the five crystal structures. The wild-type PR and mutants PR_{I84V} and PR_{V82A} had almost identical hydrogen bond interactions with SQV, except that the hydroxyl of SQV was located more asymmetrically with respect to the side chains of catalytic Asp25 and 25′ in the mutant complexes [Fig. 1(C)]. The distances from O4 to OD1, OD2 of Asp25 and Asp25′ are 2.6, 3.1, 2.9, and 2.6 Å in the mutants compared to 2.8, 2.9, 2.9, and 2.9 Å in the PR/SQV structure. Consequently, the N4 and O3 atoms of P2 were about 0.2 Å closer to residues 27–30 in the mutant structures. Both PR_{I84V} and PR_{V82A} showed small shifts in the position of the main-chain atoms at the site of mutation compared to those observed for PR [Fig. 4]. The shifts of the α-carbon of Val84 were 0.25 and 0.3 Å in the two subunits [Fig. 4(A)]. However, this movement was perpendicular to the plane of the P1′ decahydroisoquinoline ring and did not alter the overall interactions. In fact, the Ile84 side chain was located opposite to the inhibitor, and the short contacts of 84 CD1 with the carbon atoms of SQV (3.3–3.7 Å) were eliminated in the PR_{I84V} mutant and substituted by good (3.8–4.0 Å) van der Waals contacts with residues 81 and 82 [Fig. 4(A)]. The PR and PR_{I84V} had almost identical numbers of van der Waals contacts with SQV, except for the P2 position where the main chain O2 atom of SQV was 0.1–0.2 Å closer to Ile50′ of the flap in PR_{I84V}.

A shift of 0.5 Å towards SQV was observed for the α-carbon of Ala82 in both subunits of PR_{V82A} [Fig. 4(B)]. The Val82 side chain was opposite to the P1′ ring and was farther from SQV (4.3–4.9 Å interatomic distances) in the PR structure than was the side chain of Ala82 in the mutant. The CB atom of Ala82 had moved 0.2 Å nearer to the P1′ group, although the interatomic distances were still over 4.0 Å. Instead, the Pro81 shifted to form van der Waals contacts of 3.7–4.0 Å with the carbon atoms of the decahydroisoquinoline group of SQV [Fig. 4(B)], which were 0.3 Å shorter compared with those of PR. The movement of Ala82 in the other subu-

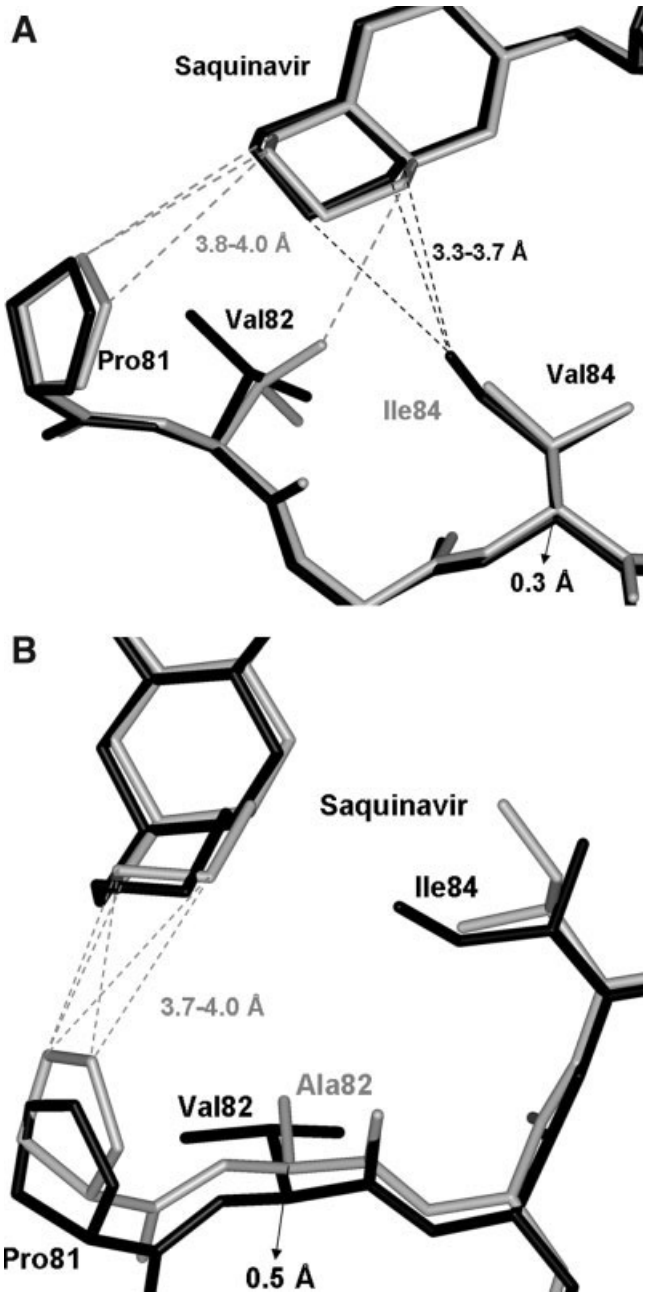

Fig. 4. Structural changes at residues 82–84 in mutant complexes compared to PR/SQV. Structure of PR/SQV is colored black while that of mutant is grey. (**A**) PR_{I84V}/SQV compared to PR/SQV. (**B**) PR_{V82A}/SQV compared to PR/SQV.

nit allowed 0.1–0.2 Å closer interactions with the P1 benzene ring. Similar movements of Ala82 in PR_{V82A} compared to Val82 in PR have been reported for the complexes with substrate analogs or darunavir.[19,20] In those structures, the shifts partially compensated for the loss of van der Waals interactions between Ala82 and inhibitor caused by the absence of the two methyl groups of Val. No such compensating interactions were observed for SQV. All these observations suggest that the mutations to smaller amino acids at residues 82 and 84 provided more space for the mutants to accommodate the larger groups of SQV. The observed minor structural adaptation of the mutants to accommodate SQV was consistent with the very similar inhibition constants observed for mutants and PR.

Comparison of PR/SQV and PR/DRV

The PR complexes with SQV and darunavir were compared in order to understand how PR binds the two different inhibitors. Both darunavir and SQV have a central hydroxyl group that forms strong hydrogen bonds with all four carboxylate oxygens of catalytic Asp25 and Asp25′. Both inhibitors share a water-mediated interaction with the flaps. Darunavir[15,19] formed seven other direct hydrogen bonds with PR, including six with the main-chain and side-chain atoms of Asp29 and Asp30/30′ [Fig. 3(B)]. In contrast, SQV showed three direct and one water-mediated hydrogen bond concentrated at one end of the inhibitor (P2 and P3), including only two interactions with Asp29/30 [Fig. 3(A)]. The hydrogen bond between the amide of SQV and the carbonyl oxygen of Gly48, which was absent in the structure of PR/DRV, was similar to the interactions observed for substrate analogs at the P2 position.[20] Hydrophobic interactions dominated in PR/SQV. SQV has larger hydrophobic groups at P1 and P1′ that provide more van der Waals interactions with PR than that observed for darunavir (99 contacts of less than 4.0 Å for PR/SQV compared to 91 for PR/DRV). The first generation PR inhibitor SQV was designed to mimic the hydrophobic interactions between substrate and PR, whereas the design goal for darunavir was to reduce its susceptibility to mutations by making new hydrogen bonds to the main-chain atoms of PR.[4,19]

To accommodate the large decahydroisoquinoline ring at P1′ of SQV, the 80s loop of residues 79–82 has undergone a conformational change by comparison to its position in the PR/DRV structure (Fig. 5). The 80s loop has moved away from the decahydroisoquinoline ring with a 1.7 Å shift of the nitrogen atom of Pro81. Due to this structural adjustment, Pro81 formed favorable van der Waals contacts at distances of 3.9–4.2 Å with the tip of the P1′ ring. The other subunit was different; the residues 79′–82′ have adopted two conformations with relative occupancy of 51%/49%. The major conformation has shifted by 0.8 Å compared with the corresponding region of PR/DRV and established 3.8–4.0 Å favorable contacts with the atoms at the tip of the P1 phenylalanine group of SQV. In the conformation with 49% population, the nitrogen atom of Pro81′ was 1.8 Å away from its position in the PR/DRV complex, which was comparable to the position described for the other subunit, and interacted with the big P1′ ring of the minor conformation of SQV with interatomic distances of 3.6–4.0 Å. Two alternate conformations of residues 79′–82′ in one subunit were observed in PR/SQV and both mutant structures, while the other subunit showed two conformations only in the PR_{V82A}/SQV complex [Fig. 1(B)]. The darunavir com-

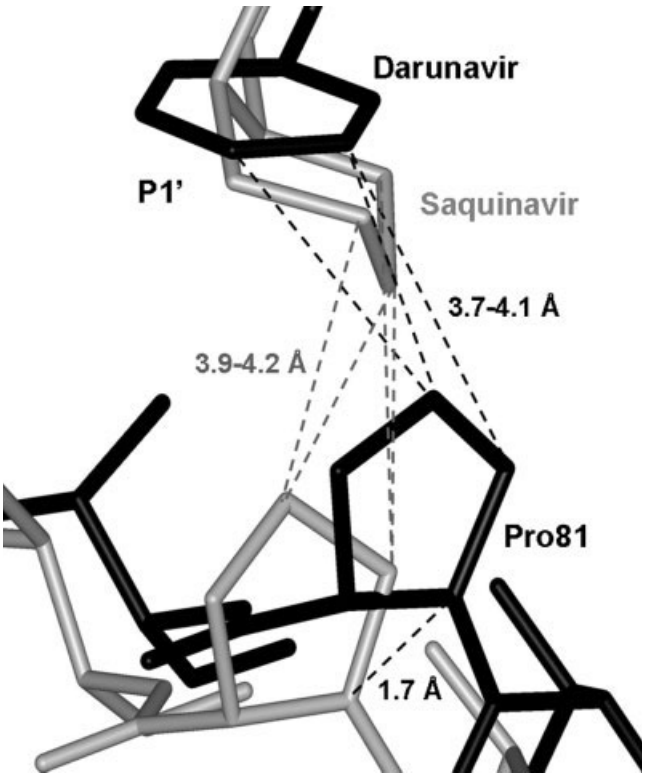

Fig. 5. Comparison of P1′ and S1′ residues in PR/SQV and PR/DRV structures. The structure of PR/DRV is colored in black bonds, while PR/SQV is grey.

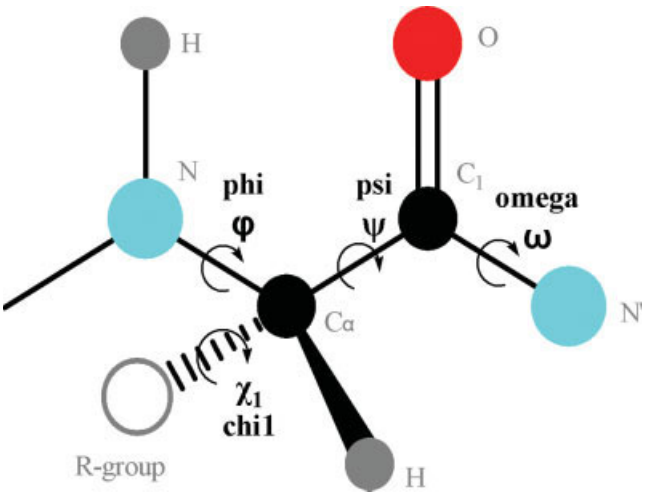

Fig. 6. Definition of the dihedral angles of protein backbone. [Color figure can be viewed in the online issue, which is available at www.interscience.wiley.com.]

TABLE II. Comparison of PR_{V82A}/SQV Complex in the Space Groups $P2_12_12_1$ and $P2_12_12$

	Average change for all residues (in deg)			
	ψ	ϕ	ω	χ1
Excluding 37–41/37′–41′	3.67	4.20	2.40	8.22
Including 37–41/37′–41′	4.27	4.53	2.49	9.34

plexes show a single conformation for the 80s loop, with little positional variation except for PR_{V82A}/DRV.[15,19] This comparison suggests that the 80s loop is intrinsically flexible and its conformation is influenced more by the properties of the inhibitor than by the PR mutations in this loop.

Comparison of the Structures in Two Different Space Groups

Since the two mutant complexes were crystallized in both the $P2_12_12$ and $P2_12_12_1$ space groups, it was possible to analyze the structural differences due to different packing in the two crystal lattices. The structures of PR_{V82A}/SQV and PR_{I84V}/SQV in the two space groups showed RMS deviations on alpha carbons of 0.7 and 0.5 Å, respectively. There were no major differences in the PR interaction with SQV in the two space groups, and the active site residues showed a very low RMS deviation of 0.1 Å. The biggest difference was for the surface residues 37–42, where the RMS deviation was over 1 Å. This region has lattice contacts with a symmetry-related molecule in the $P2_12_12$ space group but not in the other space group. The flexibility of this loop did not affect the overall packing of the PR. The other major difference was that the residues 78′–82′ in the $P2_12_12$ structure had a single conformation, whereas this region of the structure in $P2_12_12_1$ had two alternate conformations. This comparison confirmed that the differences induced by lattice packing are mainly on the protein surface and have little effect on the details of PR–inhibitor interactions.

Torsion angles were calculated for each residue in the PR_{V82A}/SQV complex and compared for the structures in the space groups $P2_12_12$ and $P2_12_12_1$ with different unit cells in order to study the flexibility and packing of each PR residue. The dihedral angles of the backbone (Fig. 6) and specific main-chain hydrogen bond interactions are typically the key to protein folding. The observed range of the torsion angles and the rotational degrees of freedom provide valuable information to apply in molecular models and predictions of protein structures. The average change in main chain φ, ψ, and ω torsion angles, and side chain χ1 torsion angle for all residues in the PR_{V82A}/SQV complex in the two space groups is given in Table II. The average changes were 3–4.5°, 2.5°, and 8°–10° for φ/ψ, ω, and χ1 angles, respectively. The dihedral φ and ψ angles of the main chain were more restricted than the χ angles of the side chain, yet there was some variation. The difference in φ angle for residues Leu38 and Gly40′ in the structures in the different space groups was over 50°, while other residues had differences of less than 20°. As mentioned above, the loop of residues 37–42 is located at the "shoulder" position leading to the flap of the PR and showed the biggest RMS deviation between the structures in the two space groups. About 9% of the residues had differences (in φ angle) of

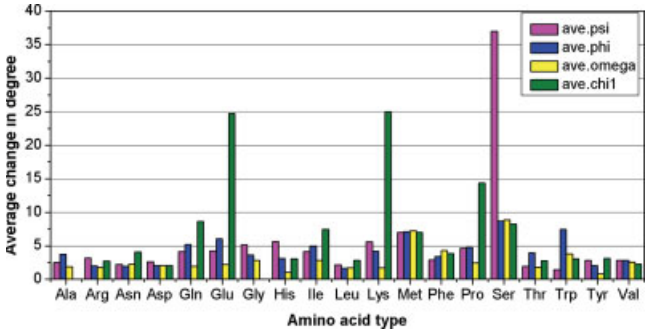

Fig. 7. Average deviation of torsion angle for different amino acid types between the PR_{V82A}/SQV structures in the two space groups $P2_12_12$ and $P2_12_12_1$. [Color figure can be viewed in the online issue, which is available at www.interscience.wiley.com.]

10–20° and most of these were located at the protein surface. Another 18% residues differed by 5–10° and were located at various positions: the dimer interface at both termini, the flaps and the residues in contact with the SQV, such as residues 28–31 and 80–82. The plots of differences in φ angles and in ψ angles for each residue had similar shapes and distributions, which suggested that the changes in the two angles were coupled. Again, residue Ser37 had the biggest difference in ψ angle of 68°, while Leu38′ and Pro39′differed by about 25°, and all other residues varied by less than 20°. The big variation in φ and ψ angles of loop 37–42 was correlated with its different lattice contacts in the two space groups. In $P2_12_12_1$, this loop interacts with residues within the same dimer, while in $P2_12_12$ it forms hydrogen bonds with a symmetry-related dimer. Around 10% residues had difference (in ψ angle) of 10–20° and 20% residues had differences of 5–10°. There was less deviation in omega angles, where the change for all residues was below 30°. About 98% of PR residues showed difference of less than 10° in the omega angle; the exceptions were Met36/36′, Ile64, and Gly49′.

The χ1 torsion angle of the side chain was much more flexible than the main-chain dihedral angles. About 10% of the residues had differences of over 20°. A plot of the average change in torsion angles against amino acid type (excluding the loops 37–41/37′–41′ which were involved in different lattice packing interactions) (Fig. 7) proved that the χ1 angle had the largest deviation, especially for residues with long side chains, such as Glu and Lys, and some hydrophobic residues, such as Pro and Ile. For residues at the protein surface with distinctly different χ1 angles, for example: loop residues 37–42, flap residue Lys55, and turn 64–65, the side chains can be perpendicular to each other or even flipped by 180°, depending on the environment (see examples in Fig. 8). The difference in χ1 angle between structures in the two space groups was in the range of 0–15° for the core residues of the protein. The most important feature is that the changes in the χ1 angle showed no correlation with the changes in the ψ and φ angles. The χ1 angle appears to depend more on the

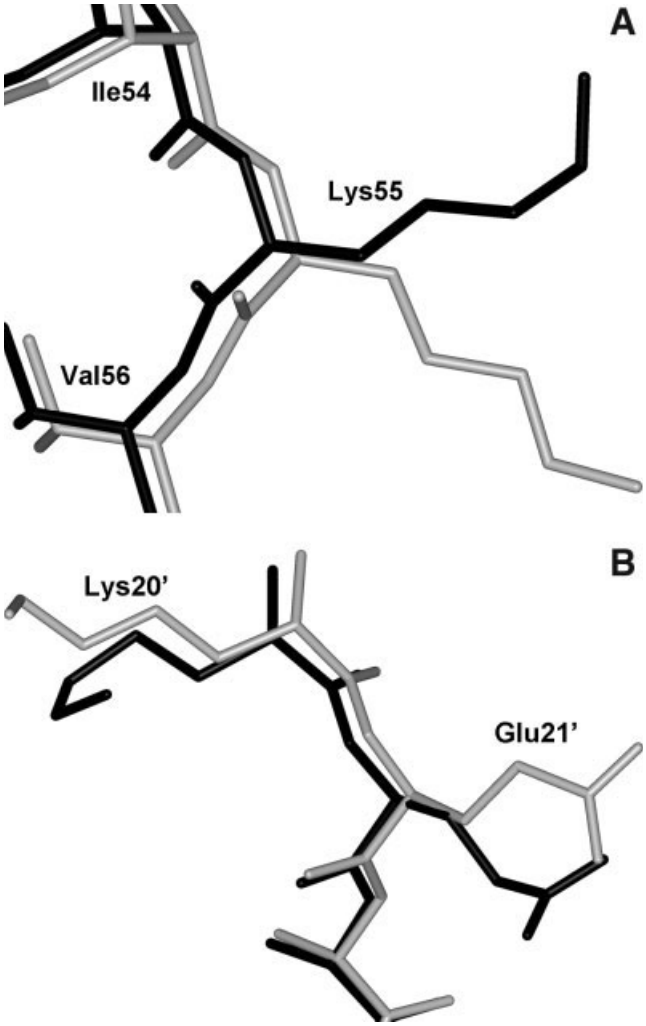

Fig. 8. Different side chain orientations of same residue for PR_{V82A}/SQV in two space groups ($P2_12_12$ and $P2_12_12_1$). The position in $P2_12_12_1$ is colored in black bonds, while that in $P2_12_12$ is in grey. (**A**) Lys55, (**B**) Glu21′.

property of the amino acid and its chemical environment. Met was the only amino acid that had very similar and relatively high changes in all four studied torsion angles. However, this result may not be significant since there are only four methionines in HIV-1 PR.

Comparison of the torsion angles for the structures solved in two space groups suggested that structural flexibility is an important feature of the PR and may be essential to its function. This analysis defines the freedom in torsion angles that should be applied during the process of molecular modeling.

Comparison With Other SQV Complexes

The PR/SQV, PR_{V82A}/SQV, and PR_{I84V}/SQV structures were compared with the published four structures of HIV PR complexes with SQV: 1HXB (wild-type PR), 1MTB ($PR_{D25N/V82A}$), 1FB7 ($PR_{G48V/L90M}$), and 1C6Z

(PR_{9X} mutant).[21–24] The PR sequence differed in six amino acids in addition to the listed point mutations. Overall, the RMS differences were 0.4–0.7 Å for main chain atoms, as usually observed for PR crystal structures in different space groups. Major differences were observed at both termini and for residues 16–18, 35–42, and 66–71, which are three turns located at the surface of the PR. Similar positions were observed for residues 79–82/79′–82′ (80s loop) and residues 42′–48′ (part of one flap) in all nine SQV complexes, which further confirmed that the large P1′ group of SQV was the major cause for the differences in the 80s loop compared to its conformation in complexes with darunavir. Moreover, SQV complexes with PR_{V82A} or the $PR_{D25N/V82A}$ (1MTB) inactive mutant had similar structural differences as described for the complexes with peptide analogs.[20] The hydroxyl oxygen of SQV was 0.23 Å closer to the catalytic Asp25/25′ than to Asn25/25′.

DISCUSSION

These new atomic resolution structures have revealed details of the PR–SQV interactions and the structural changes in the presence of mutations or between different space groups. The PR interactions with SQV, the first FDA-approved anti-HIV drug, can be compared to those with peptide analogs or newer clinical inhibitors like darunavir. There were three direct and three water-mediated hydrogen bonds between SQV and PR (excluding four from the hydroxyl group of the inhibitor to the catalytic Asp25/25′), and most were located at the P3–P2 end of SQV. The van der Waals interactions appeared to be the major contribution for SQV binding to PR. The binding affinity is determined by the Gibbs energy equation and depends on the enthalpy (ΔH) and entropy (ΔS) changes. Either making ΔH more negative or ΔS more positive will improve the PR–inhibitor binding affinity. SQV binding to HIV-1 PR is enthalpically unfavorable and is driven by the large favorable entropy change.[36] The big rigid hydrophobic groups of SQV tend to maximize the gain in desolvation entropy with a small loss in conformational entropy due to the burial of these hydrophobic groups in the active site pocket. Newer antiviral PR inhibitors, such as darunavir, were designed to enhance the strong and favorable hydrogen bonds with the main chain atoms of the PR. Darunavir shows six direct hydrogen bonds with main chain PR atoms and has enthalpically favorable binding to PR with less dependence on the entropy.[37] This design may also improve the specificity and provide better water solubility. Ideally, the inhibitor design should combine the two approaches, maintaining good hydrogen bonds with main chain atoms and improving the van der Waals contacts in the PR subsites, in order to provide tight binding and more effective inhibitors. In agreement with Ref. 36, balancing the enthalpically favorable polar interactions and desolvation entropy induced by hydrophobic groups will optimize the PR–inhibitor binding affinity and specificity.

Comparison of the structures has helped to understand why V82A and I84V are not the major drug-resistant mutations observed on exposure to SQV. Shifts of 0.3 and 0.5 Å on the alpha carbon atom of the mutated residue were observed for PR_{I84V} and PR_{V82A}, respectively, compared to the positions in wild-type PR. These changes did not significantly alter the PR–SQV interactions. The major difference at the active site was that the hydroxyl group on SQV was located more asymmetrically between the side chains of catalytic Asp25 and 25′ in the mutant complexes. The observed minor structural changes in SQV complexes were consistent with the closely similar inhibition constants of mutants and PR. In contrast, other inhibitors have shown reduced inhibition and fewer interactions with mutant compared to wild-type PR. In these SQV complexes, the mutation from bigger to smaller amino acids allows more space to accommodate the bigger side chain at P1′ of SQV.

The P1′ decahydroisoquinoline group of SQV is very big for the S1′ binding site. Compared to PR/DRV, the residues 79–82 have moved away from the active site while the residues 79′–82′ have adopted two conformations in order to accommodate the big groups of SQV. The analysis further revealed that the 80s loop of residues 79–82 is intrinsically flexible. The same shifts of the 80s loop relative to darunavir complexes were observed for all three structures, PR, PR_{V82A} and PR_{I84V}, and for structures in both the $P2_12_12$ and $P2_12_12_1$ space groups, suggesting that these structural movements were evidence of the flexible nature of the PR rather than a consequence of crystal lattice packing effects. Similar flexibility of this region was described for the 9X mutant structure.[24] Other flexible areas in the PR have been suggested, such as the residues 15–21, the 30s loop, the flap region and both termini.[38–41] The flexibility of the PR structure may play an important role in its function in viral replication.[42,43] Analysis of the non-active-site mutations, for example, mutations in the flap or dimer interface, has shown that altering these flexible regions of HIV-1 PR can influence the binding of inhibitors or substrates.[16,44]

The subatomic resolution structure of PR_{V82A}/SQV has provided greater structural detail and more accurate atomic positions to understand the subtle structural changes induced by one single mutation. The structural comparison of SQV and darunavir complexes illuminates the potential strategies to overcome drug resistance and will be valuable in developing more potent antiviral drugs.

ACKNOWLEDGMENTS

We thank the staff at the SER-CAT beamline at the Advanced Photon Source, Argonne National Laboratory for assistance during X-ray data collection. Use of the Advanced Photon Source was supported by the US Department of Energy, Basic Energy Sciences, Office of Science, under Contract No. W-31-109-Eng-38. This research was supported, in part, by the Molecular Basis

of Disease Fellowship (Y.T.), the Georgia Cancer Coalition Distinguished Cancer Scholar award (I.T.W. and R.W.H.), and the Georgia Research Alliance.

REFERENCES

1. Palella FJ, Jr, Delaney KM, Moorman AC, Loveless MO, Fuhrer J, Satten GA, Aschman DJ, Holmberg SD. Declining morbidity and mortality among patients with advanced human immunodeficiency virus infection. HIV outpatient study investigators. N Engl J Med 1998;338:853–860.
2. Tozser J, Oroszlan S. Proteolytic events of HIV-1 replication as targets for therapeutic intervention. Curr Pharm Des 2003;9: 1803–1815.
3. Prejdova J, Soucek M, Konvalinka J. Determining and overcoming resistance to HIV protease inhibitors. Curr Drug Targets Infect Disord 2004;4:137–152.
4. Koh Y, Nakata H, Maeda K, Ogata H, Bilcer G, Devasamudram T, Kincaid JF, Boross P, Wang YF, Tie Y, Volarath P, Gaddis L, Harrison RW, Weber IT, Ghosh AK, Mitsuya H. A novel bis-tetrahydrofuranylurethane-containing nonpeptidic protease inhibitors (PI) UIC-94017 (TMC114) potent against multi-PI-resistant HIV in vitro. Antimicrob Agents Chemother 2003;47:3123–3129.
5. Craig JC, Duncan IB, Hockley D, Grief C, Roberts NA, Mills JS. Antiviral properties of Ro 31-8959, an inhibitor of human immunodeficiency virus (HIV) proteinase. Antiviral Res 1991;16:295–305.
6. Deminie CA, Bechtold CM, Stock D, Alam M, Djang F, Balch AH, Chou TC, Prichard M, Colonno RJ, Lin PF. Evaluation of reverse transcriptase and protease inhibitors in two-drug combinations against human immunodeficiency virus replication. Antimicrob Agents Chemother 1996;40:1346–1351.
7. Tamalet C, Pasquier C, Yahi N, Colson P, Poizot-Martin I, Lepeu G, Gallais H, Massip P, Puel J, Izopet J. Prevalence of drug resistant mutants and virological response to combination therapy in patients with primary HIV-1 infection. J Med Virol 2000;61:181–186.
8. Condra JH, Schleif WA, Blahy OM, Gabryelski LJ, Graham DJ, Quintero JC, Rhodes A, Robbins HL, Roth E, Shivaprakash M, Titus D, Yang T, Teppler H, Squires KE, Deutsch PJ, Emini EA. In vivo emergence of HIV-1 variants resistant to multiple protease inhibitors. Nature 1995;374:569–571.
9. Jacobsen H, Hanggi M, Ott M, Duncan IB, Owen S, Andreoni M, Vella S, Mous J. In vivo resistance to a human immunodeficiency virus type 1 proteinase inhibitor: mutations, kinetics, and frequencies. J Infect Dis 1996;173:1379–1387.
10. Jacobsen H, Yasargil K, Winslow DL, Craig JC, Krohn A, Duncan IB, Mous J. Characterization of human immunodeficiency virus type 1 mutants with decreased sensitivity to proteinase inhibitor Ro 31-8959. Virology 1995;206:527–534.
11. Boucher C. Rational approaches to resistance: using saquinavir. AIDS 1996;10 (Suppl 1):S15–S19.
12. Wlodawer A, Erickson JW. Structure-based inhibitors of HIV-1 protease. Annu Rev Biochem 1993;62:543–585.
13. Wlodawer A, Vondrasek J. Inhibitors of HIV-1 protease: a major success of structure-assisted drug design. Annu Rev Biophys Biomol Struct 1998;27:249–284.
14. Kovalevsky AY, Liu F, Leshchenko S, Ghosh AK, Louis JM, Harrison RW, Weber IT. Ultra-high resolution crystal structure of HIV-1 protease mutant reveals two binding sites for clinical inhibitor TMC114. J Mol Biol 2006;363:161–173.
15. Kovalevsky AY, Tie Y, Liu F, Boross PI, Wang YF, Leshchenko S, Ghosh AK, Harrison RW, Weber IT. Effectiveness of nonpeptide clinical inhibitor TMC-114 on HIV-1 protease with highly drug resistant mutations D30N, I50V, and L90M. J Med Chem 2006;49:1379–1387.
16. Liu F, Boross PI, Wang YF, Tozser J, Louis JM, Harrison RW, Weber IT. Kinetic, stability, and structural changes in high-resolution crystal structures of HIV-1 protease with drug-resistant mutations L24I, I50V, and G73S. J Mol Biol 2005;354:789–800.
17. Liu F, Kovalevsky AY, Louis JM, Boross PI, Wang YF, Harrison RW, Weber IT. Mechanism of drug resistance revealed by the crystal structure of the unliganded HIV-1 protease with F53L mutation. J Mol Biol 2006;358:1191–1199.
18. Mahalingam B, Wang YF, Boross PI, Tozser J, Louis JM, Harrison RW, Weber IT. Crystal structures of HIV protease V82A and L90M mutants reveal changes in the indinavir-binding site. Eur J Biochem 2004;271:1516–1524.
19. Tie Y, Boross PI, Wang YF, Gaddis L, Hussain AK, Leshchenko S, Ghosh AK, Louis JM, Harrison RW, Weber IT. High resolution crystal structures of HIV-1 protease with a potent non-peptide inhibitor (UIC-94017) active against multi-drug-resistant clinical strains. J Mol Biol 2004;338:341–352.
20. Tie Y, Boross PI, Wang YF, Gaddis L, Liu F, Chen X, Tozser J, Harrison RW, Weber IT. Molecular basis for substrate recognition and drug resistance from 1.1 to 1.6 angstroms resolution crystal structures of HIV-1 protease mutants with substrate analogs. FEBS J 2005;272:5265–5277.
21. Krohn A, Redshaw S, Ritchie JC, Graves BJ, Hatada MH. Novel binding mode of highly potent HIV-proteinase inhibitors incorporating the (*R*)-hydroxyethylamine isostere. J Med Chem 1991; 34:3340–3342.
22. Prabu-Jeyabalan M, Nalivaika EA, King NM, Schiffer CA. Viability of a drug-resistant human immunodeficiency virus type 1 protease variant: structural insights for better antiviral therapy. J Virol 2003;77:1306–1315.
23. Hong L, Zhang XC, Hartsuck JA, Tang J. Crystal structure of an in vivo HIV-1 protease mutant in complex with saquinavir: insights into the mechanisms of drug resistance. Protein Sci 2000;9:1898–1904.
24. Munshi S, Chen Z, Yan Y, Li Y, Olsen DB, Schock HB, Galvin BB, Dorsey B, Kuo LC. An alternate binding site for the P1-P3 group of a class of potent HIV-1 protease inhibitors as a result of concerted structural change in the 80s loop of the protease. Acta Crystallogr 2000;56 (Part 4):381–388.
25. FDA approves new HIV treatment for patients who do not respond to existing drugs. US Food and Drug Administration (FDA), 2006.
26. Louis JM, Wondrak EM, Copeland TD, Smith CA, Mora PT, Oroszlan S. Chemical synthesis and expression of the HIV-1 protease gene in *E. coli*. Biochem Biophys Res Commun 1989; 159:87–94.
27. Wondrak EM, Louis JM. Influence of flanking sequences on the dimer stability of human immunodeficiency virus type 1 protease. Biochemistry 1996;35:12957–12962.
28. Bagossi P, Kadas J, Miklossy G, Boross P, Weber IT, Tozser J. Development of a microtiter plate fluorescent assay for inhibition studies on the HTLV-1 and HIV-1 proteinases. J Virol Methods 2004;119:87–93.
29. Otwinowski Z, Minor W. Processing of X-ray diffraction data in oscillation mode. Methods Enzymol 1997;276:307–326.
30. Navaza J. AMoRe: An automated package for molecular replacement. Acta Crystallogr A 1994;50:157–163.
31. Sheldrick GM, Schneider TR. SHELXL: High resolution refinement. Methods Enzymol 1997;277:319–343.
32. Jones TA, Zou JY, Cowan SW, Kjeldgaard M. Improved methods for building protein models in electron density maps and the location of errors in these models. Acta Crystallogr A 1991;47:110–119.
33. Esnouf RM. Further additions to MolScript version 1.4, including reading and contouring of electron-density maps. Acta Crystallogr D: Biol Crystallogr 1999;55:938–940.
34. Gulnik SV, Suvorov LI, Liu B, Yu B, Anderson B, Mitsuya H, Erickson JW. Kinetic characterization and cross-resistance patterns of HIV-1 protease mutants selected under drug pressure. Biochemistry 1995;34:9282–9287.
35. Klabe RM, Bacheler LT, Ala PJ, Erickson-Viitanen S, Meek JL. Resistance to HIV protease inhibitors: a comparison of enzyme inhibition and antiviral potency. Biochemistry 1998;37:8735–8742.
36. Velazquez-Campoy A, Todd MJ, Freire E. HIV-1 protease inhibitors: enthalpic versus entropic optimization of the binding affinity. Biochemistry 2000;39:2201–2207.
37. King NM, Prabu-Jeyabalan M, Nalivaika EA, Wigerinck P, de Bethune MP, Schiffer CA. Structural and thermodynamic basis for the binding of TMC114, a next-generation human immunodeficiency virus type 1 protease inhibitor. J Virol 2004;78:12012–12021.
38. Ishima R, Freedberg DI, Wang YX, Louis JM, Torchia DA. Flap opening and dimer-interface flexibility in the free and inhibitor-bound HIV protease, and their implications for function. Struct Fold Des 1999;7:1047–1055.

39. Rose RB, Craik CS, Stroud RM. Domain flexibility in retroviral proteases: structural implications for drug resistant mutations. Biochemistry 1998;37:2607–2621.
40. Swairjo MA, Towler EM, Debouck C, Abdel-Meguid SS. Structural role of the 30's loop in determining the ligand specificity of the human immunodeficiency virus protease. Biochemistry 1998; 37:10928–10936.
41. Zoete V, Michielin O, Karplus M. Relation between sequence and structure of HIV-1 protease inhibitor complexes: a model system for the analysis of protein flexibility. J Mol Biol 2002;315:21–52.
42. Piana S, Carloni P, Parrinello M. Role of conformational fluctuations in the enzymatic reaction of HIV-1 protease. J Mol Biol 2002; 319:567–583.
43. Piana S, Carloni P, Rothlisberger U. Drug resistance in HIV-1 protease: flexibility-assisted mechanism of compensatory mutations. Protein Sci 2002;11:2393–2402.
44. Olsen DB, Stahlhut MW, Rutkowski CA, Schock HB, vanOlden AL, Kuo LC. Non-active site changes elicit broad-based cross-resistance of the HIV-1 protease to inhibitors. J Biol Chem 1999; 274:23699–23701.